ACS OMEGA

Article

Cite This: ACS Omega 2019, 4, 22197−22202

http://pubs.acs.org/journal/acsodf

$Rb_3Na(H_2C_3N_3O_3)_4{\cdot}3H_2O$ with Large Birefringence

Mukeremu Aibibula,[†] Li Wang,*[,†] and Shuzhao Huang[‡]

[†]College of Chemistry and Chemical Engineering, Xinjiang Normal University, 102 Xinyi Road, Shayibage District, Urumqi 830054, P. R. China

[‡]Key Laboratory for Green Processing of Chemical Engineering of Xinjiang Bingtuan, School of Chemistry and Chemical Engineering, Shihezi University, 221 Beisi Road, Shihezi University Central District, Shihezi 832003, P. R. China

Supporting Information

ABSTRACT: A mixed alkali-metal nonlinear optical (NLO) dihydro-cyanurate crystal $Rb_3Na(H_2C_3N_3O_3)_4{\cdot}3H_2O$ has been synthesized via the hydrothermal method. Its calculated birefringence is about 0.368, which is very large, its ultraviolet (UV) cutoff edge is down to 230 nm, and the powder second harmonic generation (SHG) intensity is about 0.2 × KDP. In addition, a first-principles investigation of the electronic properties on $Rb_3Na(H_2C_3N_3O_3)_4{\cdot}3H_2O$ was carried out. The calculated band gap and SHG coefficient values agree well with the experimental ones. These results suggest that it could be applied as a UV birefringent material.

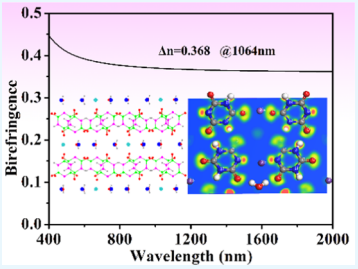

1. INTRODUCTION

Birefringence is one of the standards for the materials in which a beam of light propagating in an anisotropic crystal splits into two beams with different polarization directions and refractive indices.[1−4] The materials with suitable birefringence have been explored continuously.[5−16] Recently, numerous scientific endeavors have been made to find new birefringent materials with good nonlinear optical (NLO) performance,[17−21] and these studies suggest that the molecular construction by using large π-conjugated anionic groups like $(BO_3)^{3-}$, $(B_3O_6)^{3-}$, $(NO_2)^-$, $(CO_3)^{2-}$, $(NO_3)^-$, $(HCOO)^-$, and $(C_3N_3O_3)^{3-}$ would be a very efficient way.[22−28] By exploiting these groups, a number of excellent crystals $Ca_3(BO_3)_2$,[29] $Ba_2Ca(B_3O_6)_2$,[30] $KSrCO_3F$,[31] $Ba_2NO_3(OH)_3$,[32] $K_3(COOH)_3[B(OH)_3]_2$,[33] $Ba_3(C_3N_3O_3)_2$,[34] etc. have been designed and synthesized.

It is well-known that the large π-conjugated $(B_3O_6)^{3-}$ group is a source of excellent NLO properties in materials like the famous crystal β-BaB_2O_4 (BBO).[35,36] Owing to structural similarity, the cyanurate group $(C_3N_3O_3)^{3-}$ is a good candidate for the substation of the $(B_3O_6)^{3-}$ group. In addition, hydro-isocyanurate $(HC_3N_3O_3)^{2-}$, dihydro-isocyanurate $(H_2C_3N_3O_3)^-$ were synthesized via a more easy crystal synthesis method compared to none hydrogen bonding cyanurates.[37,38] Ye's group reported $KLi(HC_3N_3O_3){\cdot}2H_2O$ with a large second harmonic generation (SHG) response that was 5.3 times that of KH_2PO_4 (KDP), and Lin's group calculated the birefringence of $Cs_3Na(H_2C_3N_3O_3)_4{\cdot}3H_2O$ with the value of 0.29 in ab principle plane at 514 nm.[39,40] During our manuscript preparation, five compounds in the isohydro- and dihydro-cyanurates family including the title compound have been reported.[41]

In our article, the single crystal of $Rb_3Na(H_2C_3N_3O_3)_4{\cdot}3H_2O$ was obtained by a mild-temperature hydrothermal method in a short synthesis period. We reported the crystal structure and measured the powder X-ray diffractometry (XRD), IR spectrum, UV−vis−NIR spectrum, thermal analysis, SHG properties, and ab initio theoretical calculations of the title compound.

2. EXPERIMENTAL AND COMPUTATIONAL METHODS

2.1. Synthesis. $Rb_3Na(H_2C_3N_3O_3)_4{\cdot}3H_2O$ was prepared via hydrothermal reaction by using RbF (1.04 g, 10 mmol), $H_3C_3N_3O_3$ (1.29 g, 10 mmol), and NaOH (0.40 g, 10 mmol). These reactants were transferred into 120 mL autoclave equipped with teflon liners (5 mL of deionized water was added) for 16 h at 190 °C, and the mixtures were cooled slowly down to room temperature. The large quantities of crystalline bulk crystals were obtained, and the yield of $Rb_3Na(H_2C_3N_3O_3)_4{\cdot}3H_2O$ was about 67% based on Rb.

2.2. Structure Determination. Single-crystal XRD data were collected on a Bruker SMART APEX II CCD detector equipped with graphite-monochromated Mo Kα radiation (λ = 0.71073 Å) and integrated with the SAINT.[42] The crystal structure was identified with programs from SHELXTL-97.[43] Final least-squares refinement on F_o^2 with data having $F_o^2 \geq 2\sigma(F_o^2)$ includes anisotropic displacement parameters for non-hydrogen atoms. The structure was inspected for missing symmetry elements with PLATON.[44] During the refinement process, we found that Na(1) and Na(1B) were in positional disorder in the structure of the compound. We restricted the sum of the ratio of Na(1) and Na(1B) as 1 and refined them by the least-square method, which can help to get better R values. The crystal data and structure refinement information are summarized in Table S1. Final atomic coordinates and

Received: October 19, 2019
Accepted: December 3, 2019
Published: December 13, 2019

DOI: 10.1021/acsomega.9b03490
ACS Omega 2019, 4, 22197−22202

equivalent isotropic displacement parameters, selected bond lengths, and angles are listed in Tables S2 and S3 in the Supporting Information (SI), respectively.

Powder XRD was performed on a Bruker D2 PHASER X-ray diffractometer. The 2θ range of 10−70° with a scan step width of 0.02° and a fixed counting time of 0.1 s/step. The experimental and calculated powder XRD patterns of the compound are presented in Figure S2.

2.3. Thermal Analysis. The thermogravimetry/differential thermal analysis (TG−DSC) curves for the $Rb_3Na(H_2C_3N_3O_3)_4{\cdot}3H_2O$ crystal were recorded with a NETZSCH STA 449C simultaneous thermal analyzer. The sample was placed in an Al_2O_3 crucible and heated at a rate of 10 °C/min in the range of 25−800 °C under inflowing nitrogen gas.

2.4. IR Spectrum Measurement. The IR spectra of $Rb_3Na(H_2C_3N_3O_3)_4{\cdot}3H_2O$ was measured on a Shimadzu IRAffinity-1 spectrometer, which was mixed with dried KBr. The IR spectra were collected in the range of 400−4000 cm^{-1} with a resolution of 2 cm^{-1}.

2.5. UV−vis−NIR Diffuse Reflectance Measurement. The UV−vis−NIR diffuse reflectance spectra of $Rb_3Na(H_2C_3N_3O_3)_4{\cdot}3H_2O$ were measured using a Shimadzu Solid Spec-3700 DUV spectrophotometer with the measurement range extending from 200 to 1400 nm at room temperature.

2.6. Theoretical Calculation Methods. Density functional theory based on electronic structure calculations were carried out with the total energy mode of CASETEP package from the Materials Studio 5.5.[45] The exchange and correlation effects were implemented via the Perdew−Burke−Ernzerhof functional[46] with the generalized gradient approximation (GGA).[47] The relations among the ionic cores and the valence electrons were depicted by norm-conserving pseudopotentials.[48] The valence electrons of title compound were calculated as Rb $4s^24p^65s^1$, Na $2s^22p^63s^1$, C $2s^22p^2$, N $2s^22p^3$, O $2s^22p^4$, and H $1s^1$. The number of plane waves included in the basis sets was determined by the cutoff energy of 750 eV for $Rb_3Na(H_2C_3N_3O_3)_4{\cdot}3H_2O$. The numerical integration of the Brillouin zone was performed using the Monkhorst−Pack 24 k-point grids of 3 × 3 × 3. The other parameters and convergent criteria were the same as the default values of the CASTEP program.

2.7. Powder Second Harmonic Generation Measurement. The SHG measurement was investigated via the Kurtz−Perry method.[49] The 1064 nm irradiation was produced via a Q-switched Nd: YAG laser. The sample was ground and sieved into distinct particle size ranges, <38−55, 55−88, 88−105, 105−150, and 150−200 μm. For comparisons, the sieved KDP samples were categorized into the same particle size ranges.

3. RESULTS AND DISCUSSION

3.1. Single-Crystal Structure. $Rb_3Na(H_2C_3N_3O_3)_4{\cdot}3H_2O$ crystallizes in non-centrosymmetric space group $Pmn2_1$ (No. 31) with unit cell parameters: a = 16.020(7) Å, b = 6.601(3) Å, c = 11.716(5) Å and Z = 2. $Rb_3Na(H_2C_3N_3O_3)_4{\cdot}3H_2O$ features two-dimensional layers consisting of π-conjugated $(H_2C_3N_3O_3)^-$ 6-membered rings. The Rb atoms are eight-coordinated to O/N atoms with two O atoms from H_2O, while the Na atoms are six-coordinated to form the NaO_6 polyhedron with two O atoms from H_2O. Unfortunately, the Na atoms are split off with the ratio of 0.843:0.157, so we mainly discussed the higher one in the structure of the compound. Interestingly, the two polyhedra form two-dimensional layer resembling "√mark" along the a-axis in Figure 1a. The isolated $(H_2C_3N_3O_3)^-$ groups form a $_\infty^2[H_2C_3N_3O_3]^-$ layer along the b-axis in Figure 1b. The Na^+ and Rb^+ cations and H_2O are filled between $_\infty^2[H_2C_3N_3O_3]^-$ layers with a certain sequence along the a-axis in Figure 1c. In addition, the positions of hydrogen bonds and water molecules in the whole structure of $Rb_3Na(H_2C_3N_3O_3)_4{\cdot}3H_2O$ is given in Figure S1 in the SI. The bond lengths and angles for $Rb_3Na(H_2C_3N_3O_3)_4{\cdot}3H_2O$ are listed in the SI.

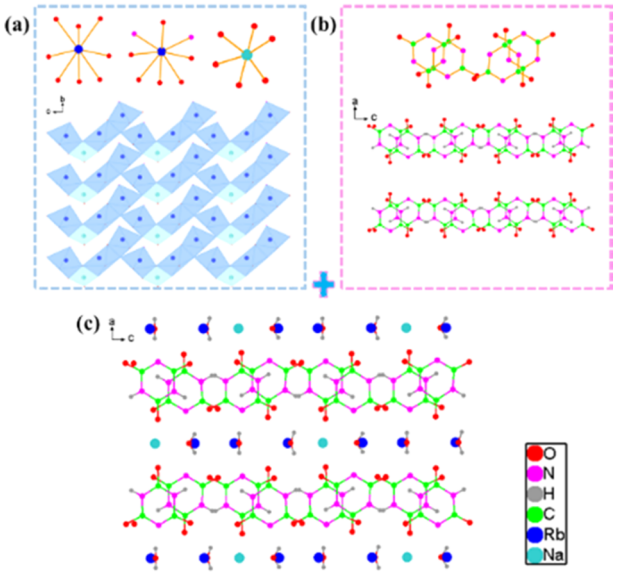

Figure 1. (a) Coordination of the Rb and Na atoms. (b) $_\infty^2[H_2C_3N_3O_3]^-$ layer with H_2O molecule. (c) Whole crystal structure of $Rb_3Na(H_2C_3N_3O_3)_4{\cdot}3H_2O$.

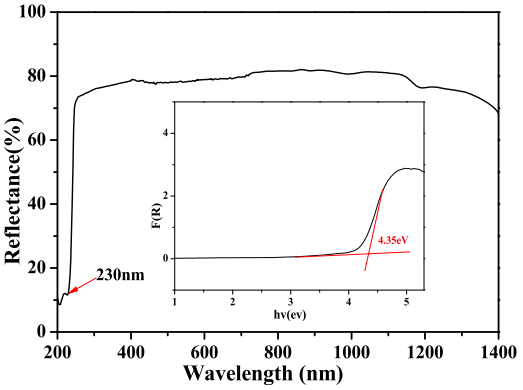

Figure 2. UV−vis−NIR diffuse reflectance spectrum for $Rb_3Na(H_2C_3N_3O_3)_4{\cdot}3H_2O$.

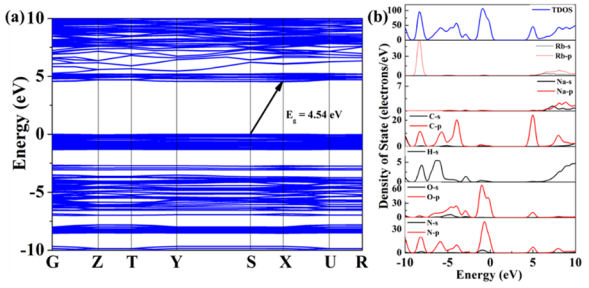

Figure 3. (a) Electronic band structure. (b) Partial density of states of $Rb_3Na(H_2C_3N_3O_3)_4{\cdot}3H_2O$.

DOI: 10.1021/acsomega.9b03490
ACS Omega 2019, 4, 22197−22202

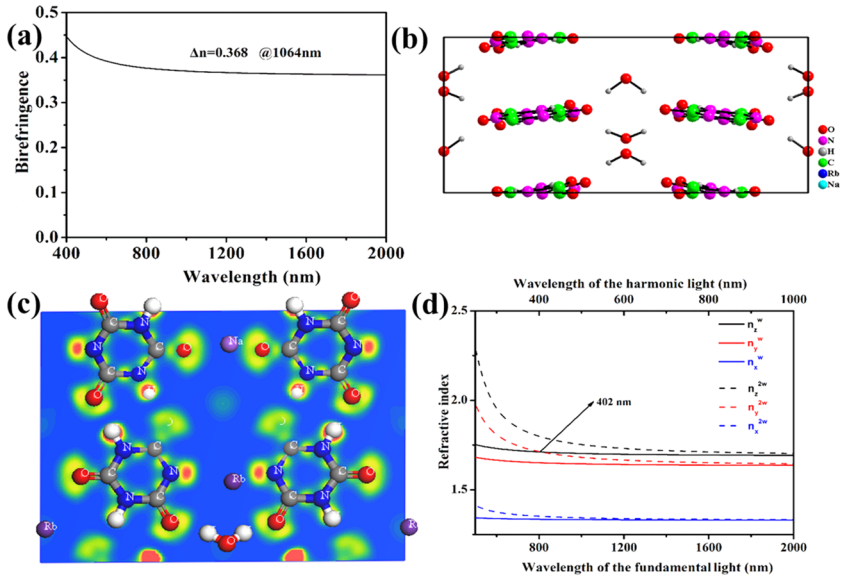

Figure 4. (a) Birefringence of $Rb_3Na(H_2C_3N_3O_3)_4{\cdot}3H_2O$. (b) (0 0 1) Direction of $Rb_3Na(H_2C_3N_3O_3)_4{\cdot}3H_2O$ in the unit cell. (c) Electron localization function map of $Rb_3Na(H_2C_3N_3O_3)_4{\cdot}3H_2O$. (d) Birefringence and accordingly predicted shortest PM wavelength.

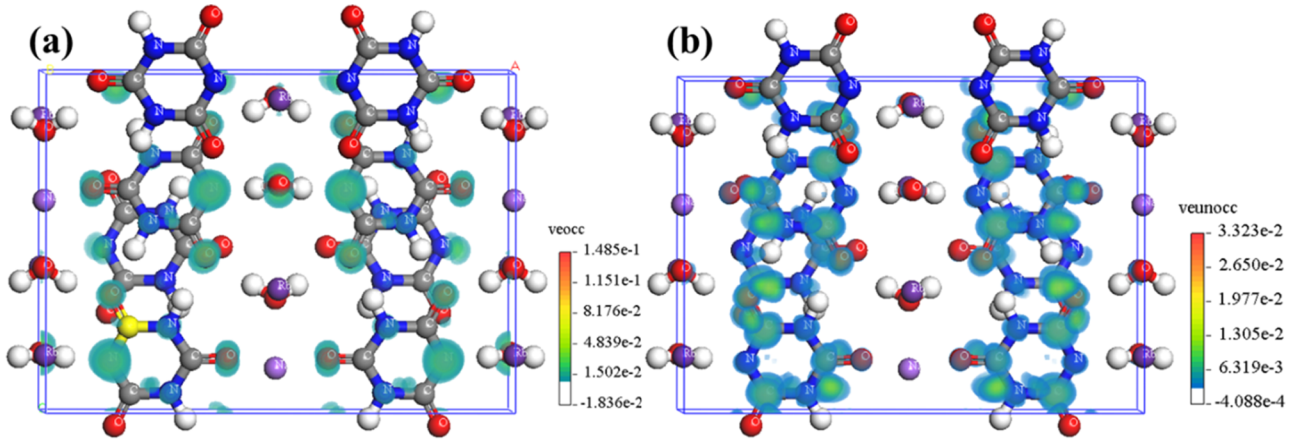

Figure 5. (a) VE occupied and (b) VE unoccupied orbitals of $Rb_3Na(H_2C_3N_3O_3)_4{\cdot}3H_2O$.

The experimental powder XRD pattern of the sample is in accordance with the theoretical one inferred from the single-crystal data (cif), implying that the obtained phase is pure (Figure S2). In addition, the distribution of Rb, Na, C, N, and O elements was certified by energy-dispersive X-ray spectroscopy (Figure S3).

3.2. IR Spectrum. The IR spectrum of $Rb_3Na(H_2C_3N_3O_3)_4{\cdot}3H_2O$ is shown in Figure S4 in the SI. The peaks around 2700−3500 cm^{-1} can confirm the presence of O−H and N−H bonds. The absorption bands observed at 1706, 1579, and 1466 cm^{-1} are characteristics of the $(H_2C_3N_3O_3)^-$ group. The C−N, N−H, and C−O bands are located at 1380, 1250, and 1074 cm^{-1}, respectively. The peak at 883 cm^{-1} may be due to the asymmetrical stretching vibration of the C_3N_3 groups. The bands at 786 and 692 cm^{-1} are assigned to the N−C−O and and the peak at 554 cm^{-1} belongs to the C═O bands.[50,51]

3.3. UV−vis−NIR Diffuse Reflectance Measurement. The UV−vis−IR reflectance spectra of $Rb_3Na(H_2C_3N_3O_3)_4{\cdot}3H_2O$ in the range of 200−1400 nm are shown in Figure 2. Evidently, its cutoff edge is down to 230 nm, with the reflectance of 12% at 240 nm, and the energy band gap is about 4.35 eV.

3.4. Thermal Analysis. Thermal analysis (Figure S4) indicates that $Rb_3Na(H_2C_3N_3O_3)_4{\cdot}3H_2O$ has two main steps of mass loss from the TG curve. There are 10% mass losses in the first small stage in the temperature range of 150−200 °C for the loss of three crystal water molecules per formula unit. The second large stage in the temperature interval between 350 and 600 °C lost mass is about 40%, which is similar to the calculated value and can be assigned to the decomposition of the $(H_2C_3N_3O_3)^-$ groups.[52] DSC curve shows that the smaller peaks at 184 °C and the stronger peaks at 378 °C represent the endothermic peaks of water molecules and $(H_2C_3N_3O_3)^-$ groups, respectively.

3.5. Electronic Structures. To better understand the relationship between the structure and property, the first-principle calculations (density functional theory) were carried out by using the CASTEP package. $Rb_3Na(H_2C_3N_3O_3)_4{\cdot}3H_2O$ shows an indirect band gap of 4.54 eV by using the GGA method (Figure 3a). The partial density of states are drawn in Figure 3b. From Figure 3b, we can note that valence band (VB) is mainly composed of Rb sp states, C sp states, H s

DOI: 10.1021/acsomega.9b03490
ACS Omega 2019, 4, 22197−22202

states, O sp states, and N sp states. The conduction band (CB) mainly consists of Na sp states, C sp states O sp states, and N sp states. The top of the VB is composed of O p states and N sp states and the bottom of CB mainly consists of C sp states N sp states and O sp states, which manifests that the $(H_2C_3N_3O_3)^-$ groups determine the electronic structure and optical properties.

3.6. Linear Optical Properties. $Rb_3Na(H_2C_3N_3O_3)_4{\cdot}3H_2O$ has a large birefringence of 0.368 at 1064 nm (Figure 4a). The largest reflective index is in the (0 0 1) direction and the $(H_2C_3N_3O_3)^-$ groups is in parallel to the light incident direction in the unit cell (Figure 4b). Thus, the largest contribution to birefringence comes from the $(H_2C_3N_3O_3)^-$ groups. The birefringence was further investigated by using visualized total electron density and electron localized function map (Figure 4c). It can be inferred that $(H_2C_3N_3O_3)^-$ holds high electron densities owing to strong covalent C−N and C−O bond. A nonspherical symmetric density distribution is clearly presented around each N (no hydrogenation) and O atom, which is composed of umbrella-shaped N 2s lone pairs and O nonbonding 2p electrons. Six parallel p_π electrons are uniformly distributed at the C_3N_3 ring, thus corresponding to a π-conjugated group; the π-conjugated groups produce strong anisotropy to be conducive to birefringence. We also calculated the bond population of $Rb_3Na(H_2C_3N_3O_3)_4{\cdot}3H_2O$, and the result is presented in Table S4. It can be found that the bond population of the H−O, C−O, C−N, and N−H groups are in the range of 0.98−0.99, 0.6−1.06, 0.78−0.98, and 0.69−0.72, respectively. It indicates that the H−O, C−O, C−N, and N−H groups display strong covalent property. As is known to all, the covalent property is beneficial for optical anisotropy and generating large birefringence for the compounds. In conclusion, the large birefringence of $Rb_3Na(H_2C_3N_3O_3)_4{\cdot}3H_2O$ is mainly triggered by $(H_2C_3N_3O_3)^-$ π-conjugated groups. In addition, the phase-matching wavelength of $Rb_3Na(H_2C_3N_3O_3)_4{\cdot}3H_2O$ was calculated (Figure 4d). It is remarkable that the calculated type I shortest PM wavelength is about 402 nm.

3.7. NLO Properties. $Rb_3Na(H_2C_3N_3O_3)_4{\cdot}3H_2O$ crystallizes into a non-centrosymmetric space group ($Pmn2_1$, No. 31). The SHG intensity of $Rb_3Na(H_2C_3N_3O_3)_4{\cdot}3H_2O$ goes up with the increasing particle size and exhibits the final SHG intensity of about 0.2 × KDP, which indicate that the title compound is phase matchable.

In addition, the SHG coefficients (d_{ij}) of $Rb_3Na(H_2C_3N_3O_3)_4{\cdot}3H_2O$ were computed to further understand the NLO properties. The space group $Pmn2_1$ belongs to the class $mm2$ point group and possesses 2 nonzero independent SHG coefficients (d_{15} = −0.0675 pm/V, d_{33} = 0.136 pm/V) under the restriction of Kleinman symmetry. The theoretically estimated value is in good agreement with the experimental one in Figure S6 in the SI.

To further investigate the origin of the SHG effects in $Rb_3Na(H_2C_3N_3O_3)_4{\cdot}3H_2O$, the donation of individual atoms in virtual-electron (VE) transition process was computed using the SHG-density method, and the SHG-density of VE occupied (veocc) and unoccupied (veunocc) states are shown in Figure 5a,b, respectively. For the occupied state, O p and N p orbitals make a significant contribution to the SHG effect. In unoccupied states, the O p, N p, and C p orbitals make the main contribution. These results indicate that the C−O groups and the $(H_2C_3N_3O_3)^-$ π-conjugated groups are the main contributors for $Rb_3Na(H_2C_3N_3O_3)_4{\cdot}3H_2O$ with large SHG response.

4. CONCLUSIONS

In summary, the single crystal of $Rb_3Na(H_2C_3N_3O_3)_4{\cdot}3H_2O$ was obtained with the hydrothermal method in a short synthesis period. The calculated birefringence of $Rb_3Na(H_2C_3N_3O_3)_4{\cdot}3H_2O$ is about 0.368, its ultraviolet (UV) cutoff edge is down to 230 nm, the SHG intensity is about 0.2 × KDP, and phase matchable. We believe that this work could contribute to the development of the cyanurates and hydroisocyanurates.

■ ASSOCIATED CONTENT

Supporting Information

The Supporting Information is available free of charge at https://pubs.acs.org/doi/10.1021/acsomega.9b03490.

Crystal data and structure refinement; the final atomic coordinates and equivalent isotropic displacement parameters and the bond valence sum for each atom in asymmetric unit; bond lengths and angles; bond population; experimentally calculated XRD pattern; elemental analysis; IR spectrum; the TG−DSC curves; the SHG intensity (PDF)

■ AUTHOR INFORMATION

Corresponding Author

*E-mail: wangliresearch@163.com.

ORCID

Li Wang: 0000-0002-7425-6872

Notes

The authors declare no competing financial interest.

■ ACKNOWLEDGMENTS

This work is supported by the National Natural Science Foundation of China (Grant No. 51762039) and Xinjiang Xuesong Plan (Grant No. 2017XS03).

■ REFERENCES

(1) Guoqing, Z.; Xu, J.; Chen, X. D.; Zhong, H. Y.; Wang, S. T.; Xu, K.; Deng, P. Z.; Gan, F. X. Growth and Spectrum of a Novel Birefringent α-BaB_2O_4 Crystal. *J. Cryst. Growth* **1998**, *191*, 517−519.

(2) Han, S. J.; Huang, C. M.; Tudi, A.; Hu, S.; Yang, Z. H.; Pan, S. L. β-CsB_9O_{14}: A Triple-Layered Borate with Edge-Sharing BO_4 Tetrahedra Exhibiting a Short Cutoff Edge and a Large Birefringence. *Chem.- Eur. J.* **2019**, 11614.

(3) Mutailipu, M.; Zhang, M.; Wu, H. P.; Yang, Z. H.; Shen, Y. H.; Sun, J. L.; Pan, S. L. $Ba_3Mg_3(BO_3)_3F_3$ Polymorphs with Reversible Phase Transition and High Performances as Ultraviolet Nonlinear Optical Materials. *Nat. Commun.* **2018**, *9*, No. 3089.

(4) Guo, J. Y.; Tudi, A.; Han, S. J.; Yang, Z. H.; Pan, S. L. $Sn_2B_5O_9Cl$: A Material with Large Birefringence Enhancement Activated via Alkaline-earth Metal Substitution by Tin. *Angew. Chem., Int. Ed.* **2019**, 17675.

(5) Chen, X. L.; Zhang, B. B.; Zhang, F. F.; Wang, Y.; Zhang, M.; Yang, Z. H.; Poeppelmeier, K. R.; Pan, S. L. Designing an Excellent Deep-Ultraviolet Birefringent Material for Light Polarization. *J. Am. Chem. Soc.* **2018**, *140*, 16311−16319.

(6) Zhang, M.; An, D. H.; Hu, C.; Chen, X. L.; Yang, Z. H.; Pan, S. L. Rational Design via Synergistic Combination Leads to an Outstanding Deep-Ultraviolet Birefringent $Li_2Na_2B_2O_5$ Material with an Unvalued B_2O_5 Functional Gene. *J. Am. Chem. Soc.* **2019**, *141*, 3258−3264.

DOI: 10.1021/acsomega.9b03490
ACS Omega 2019, 4, 22197−22202

(7) Wu, H. P.; Yu, H. W.; Yang, Z. H.; Hou, X. L.; Pan, S. L.; Su, X.; Poeppelmeier, K. R.; Rondinelli, J. M. Designing a Deep Ultraviolet Nonlinear Optical Material with Large Second Harmonic Generation Response. *J. Am. Chem. Soc.* **2013**, *135*, 4215−4219.
(8) Wu, H. P.; Pan, S. L.; Poeppelmeier, K. R.; Li, H. Y.; Jia, D. Z.; Chen, Z. H.; Fan, X. Y.; Yang, Y.; et al. $K_3B_6O_{10}Cl$: A New Structure Analogous to Perovskite with a Large SHG Response and Deep UV Absorption Edge. *J. Am. Chem. Soc.* **2011**, *133*, 7786−7790.
(9) Shi, G. Q.; Wang, Y.; Zhang, F. F.; Zhang, B. B.; Yang, Z. H.; Hou, X. L.; Pan, S. L.; Poeppelmeier, K. R. Finding the Next Deep-Ultraviolet Nonlinear Optical Material: $NH_4B_4O_6F$. *J. Am. Chem. Soc.* **2017**, *139*, 10645−10648.
(10) Zhang, B. B.; Shi, G. Q.; Yang, Z. H.; Zhang, F. F.; Pan, S. L. Fluorooxoborates: Beryllium-Free Deep-Ultraviolet Nonlinear Optical Materials without Layered Growth. *Angew. Chem., Int. Ed.* **2017**, *56*, 3916−3919.
(11) Wang, X. F.; Wang, Y.; Zhang, B. B.; Zhang, F. F.; Yang, Z. H.; Pan, S. L. CsB_4O_6F: A Congruent-Melting Deep-Ultraviolet Nonlinear Optical Material by Combining Superior Functional Units. *Angew. Chem., Int. Ed.* **2017**, *56*, 14119−14123.
(12) Mutailipu, M.; Zhang, M.; Zhang, B. B.; Wang, L. Y.; Yang, Z. H.; Zhou, X.; Pan, S. L. $SrB_5O_7F_3$ Functionalized with $[B_5O_9F_3]^{6-}$ Chromophores: Accelerating the Rational Design of Deep-Ultraviolet Nonlinear Optical Materials. *Angew. Chem., Int. Ed.* **2018**, *57*, 6095−6099.
(13) Wang, Y.; Zhang, B. B.; Yang, Z. H.; Pan, S. L. Cation-Tuned Synthesis of Fluorooxoborates: Towards Optimal Deep-Ultraviolet Nonlinear Optical Materials. *Angew. Chem., Int. Ed.* **2018**, *57*, 2150−2154.
(14) Wu, S.; Wang, G.; Xie, J.; Wu, X.; Zhang, Y.; Lin, X. Growth of Large Birefringent α-BBO Crystal. *J. Cryst. Growth* **2002**, *245*, 84−86.
(15) Deshazer, L. G. Improved Midinfrared Polarizers Using Yttrium Vanadate. *Proc. SPIE* **2002**, *4481*, 10−16.
(16) Wu, L.; Zhang, Y.; Kong, Y. F.; Sun, T. Q.; Xu, J. J.; Chen, X. L. Structure Determination of Novel Orthoborate $NaMgBO_3$: A Promising Birefringent Crystal. *Inorg. Chem.* **2007**, *13*, 5207−5211.
(17) Li, R. K.; Ma, Y. Y. Chemical Engineering of a Birefringent Crystal Transparent in the Deep UV Range. *CrystEngComm* **2012**, *14*, 5421−5424.
(18) Zhang, H.; Zhang, M.; Pan, S. L.; Yang, Z. H.; Wang, Z.; Bian, Q.; Hou, X. L.; Yu, H. W.; Zhang, F. F.; Wu, K.; Yang, F.; Peng, Q. J.; Xu, Z. Y.; Chang, K. B.; Poeppelmeier, K. R. $Na_3Ba_2(B_3O_6)_2F$: Next Generation of Deep-Ultraviolet Birefringent Materials. *Cryst. Growth Des.* **2014**, *15*, 523−529.
(19) Zhang, Z. Z.; Wang, Y.; Li, H.; Yang, Z. H.; Pan, S. L. $BaB_8O_{12}F_2$: A Promising Deep-UV Birefringent Material. *Inorg. Chem. Front.* **2019**, *6*, 546−549.
(20) Yu, H. W.; Zhang, W. G.; Halasyamani, P. Shiv. Large Birefringent Materials, $Na_6Te_4W_6O_{29}$ and $Na_2TeW_2O_9$: Synthesis, Structure, Crystal Growth, and Characterization. *Cryst. Growth Des.* **2016**, *16*, 1081−1087.
(21) Huang, L.; Zou, G. H.; Cai, H.; Wang, S. C.; Lin, C. S.; Ye, N. $Sr_2(OH)_3NO_3$: The First Nitrate as a Deep UV Nonlinear Optical Material with Large SHG Responses. *J. Mater. Chem. C* **2015**, *3*, 5268−5274.
(22) Liang, F.; Kang, L.; Zhang, X. Y.; Lee, M. H.; Lin, Z. S.; Wu, Y. C. Molecular Construction Using $(C_3N_3O_3)^{3-}$ Anions: Analysis and Prospect for Inorganic Metal Cyanurates Nonlinear Optical Materials. *Cryst. Growth Des.* **2017**, *17*, 4015−4020.
(23) Liang, F.; Wang, N. Z.; Liu, X. M.; Lin, Z. S.; Wu, Y. C. Co-crystal $LiCl\cdot(H_3C_3N_3O_3)$: A Promising Solar-blind Nonlinear Optical Crystals with Giant Nonlinearity from Coplanar π-conjugated Groups. *Chem. Commun.* **2019**, *55*, 6257−6260.
(24) Huang, C. M.; Han, G. P.; Li, H.; Zhang, F. F.; Yang, Z. H.; Pan, S. L. A New Barium Fluorooxoborate $BaB_5O_8F\cdot xH_2O$ with Large Birefringence and Wide UV Transparency Window. *Dalton Trans.* **2019**, *48*, 6714−6717.
(25) Wang, Y.; Han, J.; Tudi, A.; Zhang, Z. Z.; Yang, Z. H.; Pan, S. L. $CO(NH_2)_2NH_4Cl$: An Ultraviolet Birefringent Material with the Conjugated C═O Groups. *CrystEngComm* **2019**, 6072.
(26) Mutailipu, M.; Zhang, M.; Zhang, B. B.; Yang, Z. H.; Pan, S. L. The First Lead Fluorooxoborate PbB_5O_8F: Achieving the Coexistence of Large Birefringence and Deep-Ultraviolet Cutoff Edge. *Chem. Commun.* **2018**, *54*, 6308−6311.
(27) Liu, Q.; Li, Z.; Wang, Y.; Su, X.; Yang, Z. H.; Pan, S. L. $LiMCO_3$ (M = K,Rb,Cs): A Series of Mixed Alkali Carbonates with Large Birefringence. *Dalton Trans.* **2017**, *46*, 6894−6899.
(28) Bian, Q.; Yang, Z. H.; Dong, L. Y.; Pan, S. L.; Zhang, H.; Wu, H. P.; Yu, H. W.; Zhao, W. W.; Jing, Q. First Principle Assisted Prediction of the Birefringence Values of Functional Inorganic Borate Materials. *J. Phys. Chem. C* **2014**, *118*, 25651−25657.
(29) Zhang, S. Y.; Wu, X.; Song, Y. T.; Ni, D. Q.; Hu, B. Q.; Zhou, T. Growth of birefringent $Ca_3(BO_3)_2$ crystals by the Czochralski method. *J. Cryst. Growth* **2003**, *252*, 246−250.
(30) Jia, Z.; Zhang, N. N.; Ma, Y. Y.; Zhao, L. W.; Xia, M. J.; Li, R. K. Top-seeded Solution Growth and Optical Properties of Deep-UV Birefringent Crystal $Ba_2Ca(B_3O_6)_2$. *Cryst. Growth Des.* **2017**, *17*, 558−562.
(31) Zhang, W.; Halasyamani, P. S. Crystal Growth and Optical Properties of a UV Nonlinear Optical Material $KSrCO_3F$. *CrystEngComm* **2017**, *19*, 4742−4748.
(32) Dong, X. H.; Huang, L.; Liu, Q. Y.; Zeng, H. M.; Lin, Z. E.; Xu, D. G.; Zou, G. H. Perfect Balance Harmony in $Ba_2NO_3(OH)_3$: A Beryllium-Free Nitrate as a UV Nonlinear Optical Material. *Chem. Commun.* **2018**, *54*, 5792−5795.
(33) He, F. F.; Wang, Q.; Liu, M. J.; Huang, L.; Gao, D. J.; Bi, J.; Zou, G. H. Hydrogen Bonding Assisted Construction of Graphite-like Deep-UV Optical Materials with Two Types of Parallel π-Conjugated Units. *Cryst. Growth Des.* **2018**, *18*, 4756−4765.
(34) Tang, J.; Liang, F.; Meng, X. H.; Kang, K. J.; Yin, W. L.; Zeng, T. X.; Xia, M. J.; Lin, Z. S.; Yao, J. Y.; Zhang, G. C.; Kang, B. $Ba_3(C_3N_3O_3)_2$: A New Phase of Barium Cyanurate Containing Parallel π-Conjugated Groups as a Birefringent Material Replacement for Calcite. *Cryst. Growth Des.* **2018**, *19*, 568−572.
(35) Kokh, A.; Popov, V.; Bekker, T.; Kononova, N.; Kokh, K.; Mokrushnikov, P. Melt-solution BBO Crystal Growth under Change of the Heat Field Symmetry and its Rotation. *J. Cryst. Growth* **2005**, *275*, 669−674.
(36) Qu, G. Y.; Hu, Z. F.; Wang, Y. P.; Yang, Q.; Tong, L. M. Synthesis of Optical-Quality Single-Crystal β-BaB_2O_4 Microwires and Nanowires. *Adv. Funct. Mater.* **2013**, *23*, 1232−1237.
(37) Wang, N. Z.; Liang, F.; Yang, Y.; Zhang, S. Z.; Lin, Z. S. A New Ultraviolet Transparent Hydra-Cyanurate $K_2(C_3N_3O_3H)$ with Strong Optical Anisotropy from Delocalized π-Bonds. *Dalton Trans.* **2019**, *48*, 2271−2274.
(38) Xia, M. J.; Liang, F.; Meng, X. H.; Wang, Y. G.; Lin, Z. S.; Intrinsic Zero, A. Thermal Expansion in Cube Cyanurate $K_6Cd_3(C_3N_3O_3)_4$. *Inorg. Chem. Front.* **2019**, *6*, 2291−2295.
(39) Lin, D. H.; Luo, M.; Lin, C. S.; Xu, F.; Ye, N. $KLi(HC_3N_3O_3)\cdot 2H_2O$: Solvent-Drop Grinding Method toward the Hydro-isocyanurate Nonlinear Optical Crystal. *J. Am. Chem. Soc.* **2019**, *141*, 3390−3394.
(40) Meng, X. H.; Liang, F.; Tang, J.; Kang, K. J.; Huang, Q.; Yin, W. L.; Lin, Z. S.; Xia, M. J. $Cs_3Na(H_2C_3N_3O_3)_4\cdot 3H_2O$: A Mixed Alkali-Metal Hydroisocyanurate Nonlinear Optical Material Containing π-Conjugated Six-Membered-Ring Units. *Eur. J. Inorg. Chem.* **2019**, 2791.
(41) Lu, J.; Lian, Y. K.; Xiong, L.; Wu, Q. R.; Zhao, M.; Shi, K. X.; Chen, L.; Wu, L. M. How to Maximize Birefringence and Nonlinearity of π-Conjugated Cyanurates. *J. Am. Chem. Soc.* **2019**, DOI: 10.1021/jacs.9b08851.
(42) *SAINT*, version 7.60A; Bruker Analytical X-ray Instruments. Inc.: Madison, WI, 2008.
(43) Sheldrick, G. M. A short history of SHELX. *Acta Crystallogr., Sect. A: Found. Crystallogr.* **2008**, *64*, 112−122.

DOI: 10.1021/acsomega.9b03490
ACS Omega 2019, 4, 22197−22202

(44) Spek, A. L. Single-crystal Structure Validation with the Program PLATON. *J. Appl. Crystallogr.* **2003**, *36*, 7−13.
(45) Clark, S. J.; Segall, M. D.; Pickard, C. J.; Hasnip, P. J.; Probert, M. J.; Refson, K.; Payne, M. C. First-principles Methods Using CASTEP. *Z. Kristallogr. - Cryst. Mater.* **2005**, *220*, 567−570.
(46) Rappe, A. M.; Rabe, K. M.; Kaxiras, E.; Joannopoulos, J. D. Optimized Pseudopotentials. *Phys. Rev. B.* **1990**, *41*, No. 1227.
(47) Perdew, J. P.; Burke, K.; Ernzerhof, M. Perdew, Burke, and Ernzerhof Reply. *Phys. Rev. Lett.* **1998**, *80*, No. 891.
(48) Lin, J. S.; Qteish, A.; Payne, M. C.; Heine, V. Optimized and Transferable Nonlocal Separable Ab Initio Pseudopotentials. *Phys. Rev. B* **1993**, *47*, No. 4174.
(49) Kurtz, S. K.; Perry, T. T. A Powder Technique for the Evaluation of Nonlinear Optical Materials. *J. Appl. Phys.* **1968**, *39*, 3798−3813.
(50) Meng, X.; Liang, F.; Tang, J.; Kang, K.; Zeng, T.; Yin, W. L.; Guo, R. X.; Lin, Z. S.; Xia, M. J. Parallel Alignment of π-Conjugated Anions in Hydroisocyanurates Enhancing Optical Anisotropy. *Inorg. Chem.* **2019**, 8948.
(51) Meng, X.; Liang, F.; Tang, J.; Kang, K.; Zeng, T.; Guo, R. X.; Lin, Z. S.; Xia, M. J. Facile Growth of an Ultraviolet Hydroisocyanurate Crystal with Strong Nonlinearity and a Wide Phase-Matching Region from π-Conjugated $(HC_3N_3O_3)^{2-}$ Groups. *Inorg. Chem.* **2019**, 11289.
(52) Meng, X.; Liang, F.; Kang, K.; Tang, J.; Huang, Q.; Yin, W. L.; Lin, Z. S.; Xia, M. J. Rich Structural Chemistry in π-Conjugated Hydroisocyanurates: Layered Structures of $A_2B(H_2C_3N_3O_3)_4{\cdot}nH_2O$ (A = K, Rb, Cs; B = Mg, Ca; n = 4, 10) with High Ultraviolet Transparency and Strong Optical Anisotropy. *Dalton Trans.* **2019**, 9048.

DOI: 10.1021/acsomega.9b03490
ACS Omega 2019, 4, 22197−22202